THE POSSIBILITY OF AN ADAPTIVE CONTROL OF COOLING-DEFROSTING CYCLE DEPENDING ON FROST CONDITIONS AT THE EVAPORATOR

Kristian Lenić*, Anica Trp, Bernard Franković
Faculty of Engineering, University of Rijeka, Vukovarska 58,
HR-51000 Rijeka, Croatia
Phone: +385 51 651 518, fax: +385 51 675 801,
E-mail: kristian.lenic@riteh.hr, anica.trp@riteh.hr, bernard.frankovic@riteh.hr

Abstract: *In the paper, an analysis of a refrigeration device operation under frost forming conditions has been performed. The results of mathematical modelling and numerical calculation of heat and mass transfer in the boundary layer have been used as a base for the calculation of an effective exchanged heat flux. Several cases with different operating conditions have been analysed and the resulting correlations for determining the optimal duration of the cooling cycle have been shown. The presented results could be used to control the device within the scope of maximising the cooling effect and reliability of a cooling energy supply. In the controlling algorithm hereunder, the starting moment of the defrosting cycle has been selected depending on real frosting conditions such as air temperature, humidity and velocity as well as temperature of the heat exchanger surface.*

Key words: fin-and-tube heat exchanger, defrosting process

1. INTRODUCTION

The frost layer, formed when an evaporator operates in moist air and when a fin surface has been cooled below 0°C, represents significant thermal resistance. Therefore, a defrosting process has to be performed, which consumes an additional amount of energy. Moreover, it causes interruptions in the cooling energy supply and leads to insertion of additional heat to the cooled space. Frost layer growth results with a reduction of mean exchanged heat flux, which can be significantly smaller than nominal heat flux exchanged on frost-free surfaces. Frost layer forming has an effect on the space cooling quality and the operating behaviour of the whole device (Sanders, 1974). For maximising the cooling efficiency it is necessary to control the device in an appropriate manner. Selection of the appropriate starting moment of the defrosting cycle is of a great importance.
Therefore, in the paper, a simulation and an analysis of the device operation during working cycles have been performed. During continuous operation the cooling cycle and defrosting cycle have been alternated in sequences. As a base for the simulation of the device operation under frost growth conditions, a detailed calculation of frost layer formation and exchanged heat flux has to be performed. The model mathematically describes the physical mechanism of frost layer forming, in which one part of the water vapour flux condenses and solidifies on a frost surface, thus increasing the frost layer thickness. The other part of the water vapour flux penetrates by diffusion into the frost layer and increases the frost density. The increase of the frost density caused by water vapour diffusion leads to augmentation of thermal conductivity and finally to reduction of thermal resistance of the frost layer. The mathematical model of heat and mass transfer during frost formation has been based on previous

investigations (Lenic et al., 2008). Many authors analysed and mathematically described the frost formation process using different levels of a mathematical and numerical approach (Lenic et al., 2008; Hayarishi et al., 1977; Lee et al., 1997; Gall et al., 1997; Lenic, 2006). In the majority of the models, the frost layer is considered as a porous structure containing iced mesh and air gaps (Tao et al., 1993; Lee ae al., 2003). Some of the models use empirical correlations on the air-side (Lee et al., 1997; Jones and Parker, 1975; Sahin, 1995; Na and Weeb, 2004). The other group of models give some improvements and analyse the air flow using boundary layer equations and predict frost properties using empirical correlations (Sherif et al., 1990; Yang and Lee, 2005). The frost forming process has also been investigated experimentally by Cheng and Shiu (2002) and Na and Weeb (2004). The most sophisticated recent models include calculation of the boundary layer using governing equations, both for the air and frost side (Hayarishi et al., 1977; Tao et al., 1993; Lee et al., 2003). Some authors analyse frost formation in a turbulent flow (Yang et al., 2006) as well as behaviour of the whole heat exchanger under frosting conditions (Yang et al., 2006; Tso et al., 2006). As in recent investigations, in the presented paper it is assumed that the partial pressure of water vapour on the frost layer surface is larger than the partial pressure of water vapour for the temperature of frost layer surface, i.e. the air near the surface of frost layer is supersaturated (Lenic et al., 2008; Lenic, 2006; Na and Weeb, 2004; Mago and Sherif, 2005; Lee and Ro, 2005). The aim of this research presented in the paper is to provide a controlling algorithm for device operation to maximise the cooling effect and reliability of cooling energy supply. The control is based on real frosting conditions: air temperature, humidity and velocity as well as temperature of the heat exchanger surface.

2. MATHEMATICAL MODEL

For simulation of exchanged heat on a fin-and-tube heat exchanger, a specific mathematical model has been used and solved numerically. The domain of calculation has been extracted from the physical model of the fin-and-tube heat exchanger and includes a representative part of the heat exchanger i.e. one half of the space between fins, as presented on Fig. 1. Two different regions which need a different mathematical approach can be distinguished: the subdomain of the humid air and subdomain of the frost layer, which are delimited by the air-frost interface. According to earlier studies, it has been assumed that the frost layer subdomain is a porous medium.
A transient two-dimensional mathematical model of frost formation has been developed. The applied mathematical model has been defined using governing equations for the boundary layer near and inside the frost layer. Governing equations and boundary conditions for both regions have been presented on Fig. 2. The presented model calculates velocity and temperature fields of the boundary layer near the cooled fin in a humid air stream, as well as the temperature and density fields inside the frost layer. It predicts a frost layer growth rate as well as a change of the thermal conductivity of the frost layer.

The exchanged heat flux has been significantly influenced by the frost layer which has formed on heat exchanger surfaces. The frost layer growth rate depends on a water vapour transfer from an air stream into the frost layer, diffusion rate of the water vapour into the frost layer and thermal conduction inside the layer. Only one part of the water vapour flux which transfers from the air stream has been deposited on the frost surface and increases the frost thickness. The other part of the water vapour flux enters e the frost layer and thus increases its density.

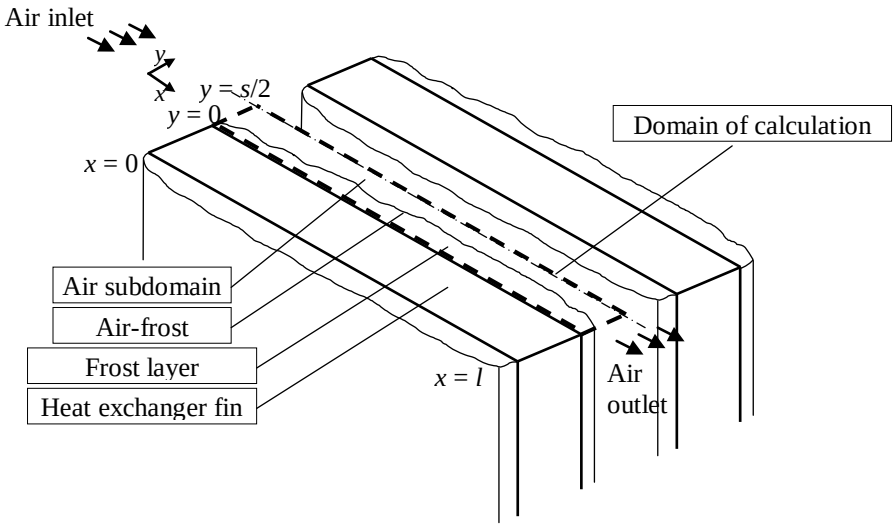

Figure 1. Domain of numerical calculation: half space between heat exchanger fins

$$\frac{\partial u_x}{\partial y}=0 \quad u_y=0 \quad \frac{\partial T_\mathrm{a}}{\partial y}=0 \quad \frac{\partial w}{\partial y}=0$$

Air inlet

$u_x = u_\mathrm{in}$

$u_y = 0$

$T_\mathrm{a} = T_\mathrm{in}$

$w = w_\mathrm{in}$

Air subdomain

$$\frac{\partial}{\partial x}\left(\rho_\mathrm{a}\, u_x\right)+\frac{\partial}{\partial y}\left(\rho_\mathrm{a}\, u_y\right)=0$$

$$\rho_\mathrm{a}\frac{\partial u_x}{\partial t}+\rho_\mathrm{a}\left(u_x\frac{\partial u_x}{\partial x}+u_y\frac{\partial u_x}{\partial y}\right)=-\frac{\partial p}{\partial x}+\mu\left(\frac{\partial^2 u_x}{\partial x^2}+\frac{\partial^2 u_x}{\partial y^2}\right)$$

$$\rho_\mathrm{a}\frac{\partial u_y}{\partial t}+\rho_\mathrm{a}\left(u_x\frac{\partial u_y}{\partial x}+u_y\frac{\partial u_y}{\partial y}\right)=-\frac{\partial p}{\partial y}+\mu\left(\frac{\partial^2 u_y}{\partial x^2}+\frac{\partial^2 u_y}{\partial y^2}\right)$$

$$\rho_\mathrm{a}\frac{\partial T_\mathrm{a}}{\partial t}+\rho_\mathrm{a}\cdot\left(u_x\frac{\partial T_\mathrm{a}}{\partial x}+u_y\frac{\partial T_\mathrm{a}}{\partial y}\right)=\frac{k_\mathrm{a}}{c_{\mathrm{p,a}}}\left(\frac{\partial^2 T_\mathrm{a}}{\partial x^2}+\frac{\partial^2 T_\mathrm{a}}{\partial y^2}\right)$$

$$\rho_\mathrm{a}\frac{\partial w}{\partial t}+\rho_\mathrm{a}\cdot\left(u_x\frac{\partial w}{\partial x}+u_y\frac{\partial w}{\partial y}\right)=\rho_\mathrm{a}\cdot D\cdot\left(\frac{\partial^2 w}{\partial x^2}+\frac{\partial^2 w}{\partial y^2}\right)$$

Air outlet

$\frac{\partial u_x}{\partial x}=0$

$\frac{\partial u_y}{\partial x}=0$

$\frac{\partial T_\mathrm{a}}{\partial x}=0$

$\frac{\partial w}{\partial x}=0$

Air-frost interface

$u_x = 0 \qquad u_y = 0$

$$k_\mathrm{a}\frac{\partial T_\mathrm{a}}{\partial y}=k_\mathrm{fl}\frac{\partial T_\mathrm{fl}}{\partial y}+q_\mathrm{sub}\rho_\mathrm{fl}\frac{\mathrm{d}y_\mathrm{fl}}{\mathrm{d}t}$$

$$\frac{\partial \rho_\mathrm{fl}}{\partial y}=0 \qquad w_\mathrm{fs}=0.622\cdot\frac{(1+S)p_{\mathrm{v,sat}}}{p-(1+S_\mathrm{v})p_{\mathrm{v,sat}}},\quad S=0.808\left(\frac{p_{\mathrm{v},\infty}}{p_{\mathrm{v,sat},\infty}}\right)\left(\frac{p_{\mathrm{v,sat,fs}}}{p_{\mathrm{v,sat},\infty}}\right)^{-0.657}-1$$

$\frac{\partial T_\mathrm{fl}}{\partial x}=0$

$\frac{\partial(\rho_\mathrm{v}/\rho_\mathrm{a})}{\partial x}=0$

Frost layer

$$\rho_\mathrm{fl}\frac{\partial T_\mathrm{fl}}{\partial t}=\frac{\partial}{\partial x}\left(\frac{k_\mathrm{fl}}{c_{\mathrm{p,fl}}}\frac{\partial T_\mathrm{fl}}{\partial x}\right)+\frac{\partial}{\partial y}\left(\frac{k_\mathrm{fl}}{c_{\mathrm{p,fl}}}\frac{\partial T_\mathrm{fl}}{\partial y}\right)+q_\mathrm{sub}\frac{\partial \rho_\mathrm{fl}}{\partial t}$$

$$\frac{\partial \rho_\mathrm{fl}}{\partial t}=\frac{\partial}{\partial x}\left(D_\mathrm{eff}\rho_\mathrm{a}\frac{\partial(\rho_\mathrm{v}/\rho_\mathrm{a})}{\partial x}\right)+\frac{\partial}{\partial y}\left(D_\mathrm{eff}\rho_\mathrm{a}\frac{\partial(\rho_\mathrm{v}/\rho_\mathrm{a})}{\partial y}\right)$$

$\frac{\partial T_\mathrm{fl}}{\partial x}=0$

$\frac{\partial(\rho_\mathrm{v}/\rho_\mathrm{a})}{\partial x}=0$

y, x

Fin surface

$$T_\mathrm{fl}=T_\mathrm{s} \qquad \frac{\rho_\mathrm{v}}{\rho_\mathrm{a}}=\frac{\rho_\mathrm{v}(T_\mathrm{s})}{\rho_\mathrm{a}(T_\mathrm{s})}$$

Figure 2. Governing equations and boundary conditions on a domain of numerical calculation

The frost layer growth rate is defined as follows:

$$\frac{\mathrm{d}y_{\mathrm{fl}}}{\mathrm{d}t} = \frac{1}{\rho_{\mathrm{fl}}}\dot{m}_{\Delta y} = \frac{1}{\rho_{\mathrm{fl}}}\left(\dot{m}_{\mathrm{a}} - \dot{m}_{\mathrm{dif}}\right) \tag{1}$$

The total mass flux of water vapour transferred from air to the frost layer surface and the mass flux which enters into frost layer by diffusion are defined respectively as follows:

$$\dot{m}_{\mathrm{a}} = \rho_{\mathrm{a}} \cdot D \cdot \frac{\mathrm{d}w}{\mathrm{d}y}, \quad \dot{m}_{\mathrm{diff}} = -\rho_{\mathrm{a}} \cdot D_{\mathrm{eff}} \cdot \frac{\mathrm{d}\left(\rho_{\mathrm{v}}/\rho_{\mathrm{a}}\right)}{\mathrm{d}y} \tag{2}$$

The above-mentioned water vapour mass fluxes have been calculated for every time step, following the calculation of the velocity, humidity, temperature and density fields. These values of water mass fluxes are used to calculate the frost growth rate. Then the overall heat transfer coefficient and, consequently, the exchanged heat flux have been obtained.

The specific heat and effective thermal conductivity of the frost layer depend on frost density, porosity and effective diffusion coefficient. They have been calculated accordingly [8, 11, 12], using following terms:

$$k_{\mathrm{fl}} = 0.132 + 3.13 \cdot 10^{-4}\rho_{\mathrm{fl}} + 1.6 \cdot 10^{-7}\rho_{\mathrm{fl}}^{\ 2} \tag{3}$$

$$c_{\mathrm{p,\,fl}} = \frac{1}{\rho_{\mathrm{fl}}}\left[\rho_{\mathrm{i}}(1-\varepsilon)c_{\mathrm{p,\,i}} + \rho_{\mathrm{a}}\varepsilon\, c_{\mathrm{p,a}}\right] \tag{4}$$

$$D_{\mathrm{eff}} = D \cdot \varepsilon \cdot \frac{1+\varepsilon}{2} \tag{5}$$

The overall heat transfer coefficient related to a segment of the fin-and-tube heat exchanger shown on Fig. 3, has been calculated using

$$U = \left[\frac{1}{U_{\mathrm{fin}}\left(\eta_{\mathrm{fin}} + \dfrac{\Delta A_{\mathrm{pipe}}}{\Delta A_{\mathrm{fin}}} \cdot \dfrac{U_{\mathrm{pipe}}}{U_{\mathrm{fin}}}\right)} + \frac{\Delta A_{\mathrm{pipe}}}{\Delta A_{\mathrm{R}}}\frac{a}{c_{\mathrm{p,a}} \cdot h_{\mathrm{R}}}\right]^{-1} \tag{6}$$

where U_{fin} and U_{pipe} denote overall heat transfer coefficients for the fin and pipe of the heat exchanger respectively and have been calculated using the following equations:

$$U_{\mathrm{fin}} = \frac{1}{\dfrac{\Delta A_{\mathrm{fin}}}{\Delta A_{\mathrm{fl,\,fin}}} \cdot \dfrac{1}{h_{\mathrm{a}}} + \dfrac{\Delta A_{\mathrm{fin}}}{\Delta \overline{A}_{\mathrm{fin}}} \cdot \overline{W}_{\mathrm{fl}}\dfrac{a}{c_{\mathrm{p,a}}}} \tag{7}$$

$$U_{\mathrm{pipe}} = \frac{1}{\dfrac{\Delta A_{\mathrm{pipe}}}{\Delta A_{\mathrm{fl,\,pipe}}} \cdot \dfrac{1}{h_{\mathrm{a}}} + \dfrac{\Delta A_{\mathrm{pipe}}}{\Delta \overline{A}_{\mathrm{pipe}}} \cdot \overline{W}_{\mathrm{fl}}\dfrac{a}{c_{\mathrm{p,a}}}} \tag{8}$$

The instantaneous exchanged heat flux on the total surface area of the heat exchanger has been calculated using

$$\dot{Q} = \frac{U}{c_{\mathrm{p,a}}}\frac{\left(h_{\mathrm{a},1} - h_{\mathrm{sat},\,T_{\mathrm{R2}}}\right) - \left(h_{\mathrm{a},2} - h_{\mathrm{sat},\,T_{\mathrm{R1}}}\right)}{\ln\dfrac{h_{\mathrm{a},1} - h_{\mathrm{sat},\,T_{\mathrm{R2}}}}{h_{\mathrm{a},2} - h_{\mathrm{sat},\,T_{\mathrm{R1}}}}}A_{\mathrm{fin,tot}} \tag{9}$$

For a limiting case, when the refrigerant temperature is assumed to be constant (approximating the evaporator) the expression for the instantaneous exchanged heat flux becomes

$$\dot{Q} = \frac{U}{c_{\mathrm{p,a}}} \left(\frac{h_{\mathrm{a},1} - h_{\mathrm{a},2}}{\ln \dfrac{h_{\mathrm{a},1} - h_{\mathrm{sat},T_{\mathrm{R}}}}{h_{\mathrm{a},2} - h_{\mathrm{sat},T_{\mathrm{R}}}}} \right) A_{\mathrm{lam,tot}} \tag{10}$$

A detailed description of the numerical approach has been given in previous works (Lenic et al. 2008.; Lenic, 2006).

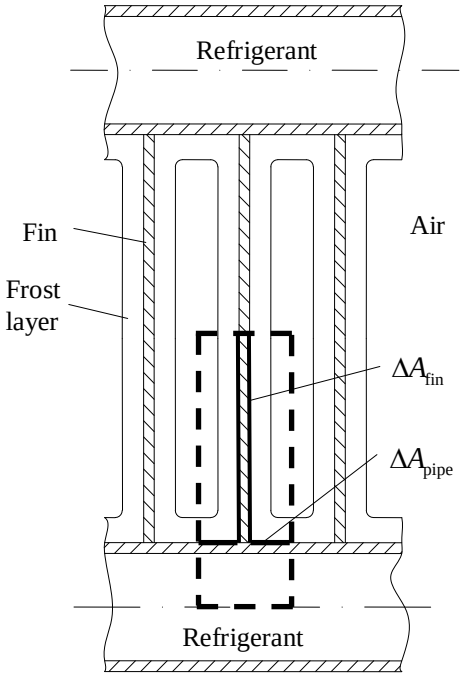

Figure 3. Elementary segment of fin-and-tube heat exchanger

A typical cycle of a chiller operation when working under frost formation conditions is shown on Fig 4. When the chiller operates under frost growth conditions, a reduction in the exchanged heat flux at the evaporator side occurs. After some time of device running, it is necessary to provide the defrosting process in order to restore the nominal exchanged heat flux. Defrosting is often very inconvenient, because long defrosting periods can result in undesirable condition changes in the cooled space. After a cooling time t_{C}, there follows the time used for defrosting t_{D}. In the presented analysis it is assumed that defrosting heat is supplied by a constant heat flux. The total duration of whole cool-defrost cycle t_{CD} is the sum of cooling and defrosting times. The nominal exchanged heat flux $\dot{Q}_0$ is provided only at the beginning of a cooling cycle, when there is no frost on the heat exchanger fins. The exchanged heat flux at the evaporator side decreases as a result of frost layer growth and increase of thermal resistance. The average exchanged heat flux during the cooling period has been calculated using

$$\overline{\dot{Q}}_{\mathrm{C}} = \frac{1}{t_{\mathrm{C}}} \int_{t_{\mathrm{C}}} \dot{Q}(t)\,\mathrm{d}t \tag{11}$$

During the defrosting process, it is necessary to provide a sufficient amount of heat for melting the whole frost layer. There are several types of defrosting techniques. The overview of defrosting types has been given in Table 1 according to Sanders (1977). Moreover, three types of control procedures have been used to control the defrosting process: Time-Initiated-

Time-Terminated, Time-Initiated-Temperature-Terminated and Time-Initiated-Pressure-Terminated defrosting control.

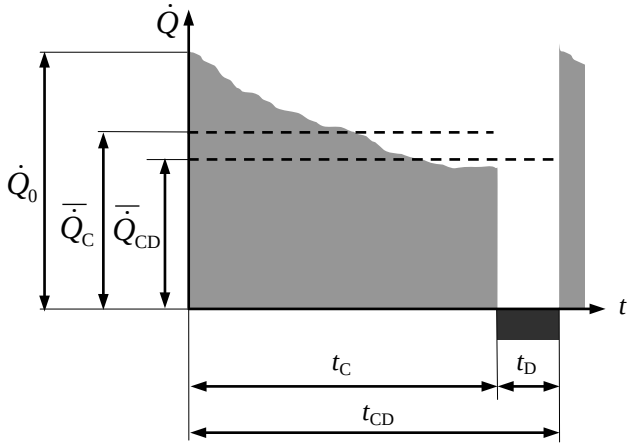

Figure 4. The typical cycle of a chiller operation during frost formation conditions

In the presented mathematical model, when modelling the defrosting process, it is assumed that the heat for defrosting is supplied from the refrigerant side i.e. from the fin side. It is also assumed that the process occurs with a constant defrosting heat flux. During the mathematical modelling the entire defrosting process is divided into two phases, which differ mainly by the heat transfer. In the first phase, the temperature of the frost layer and fins changes up to the melting temperature of water (0 °C). During the second phase, melting of the frost layer takes place. Through mathematical modelling of these two phases, the minimal heat for the defrosting process can be calculated. The minimal heat for defrosting in an ideal case, ignoring the thermal capacity of the heat exchanger, amounts:

$$Q_D = Q_{D,\min} = \int_{t_D} \dot{Q}_D(t)\,dt = m_{fl} \cdot c_{p,fl} \cdot T_D^0 + m_{fl} \cdot q_{mt} \tag{12}$$

As the defrosting process consumes energy and influences the cooling supply continuity, it is important not to continue the defrosting longer than is absolutely necessary.

The effective cooling output has been significantly affected by air humidity i.e. frost growth rate. It has been significantly influenced by the defrosting process also. The calculation of the average exchanged heat flux therefore includes a period of cooling and a defrosting period. The average exchanged heat flux i.e. effective exchanged heat flux in the heat exchanger, during the whole cycle, has been defined as

$$\overline{\dot{Q}}_{CD} = \frac{\int_{t_C} \dot{Q}(t)\,dt - \int_{t_D} \dot{Q}_D(t)\,dt}{t_C + t_D} \tag{13}$$

3. NUMERICAL CALCULATION AND VERIFICATION

In order to determine the instantaneous exchanged heat flux, a detailed calculation of boundary layer has been performed. The governing equations which describe boundary layer, presented in Fig. 2, are discretised using the control volume method. To avoid a physically unrealistic pressure field in the air subdomain, staggered grids for velocity components have been used. The convection-diffusion terms have been discretised using a power-law scheme. An iterative procedure has been used to solve the resulting set of linearised discretised equations. For the time-stepping numerical treatment, a fully implicit method has been used. A SIMPLER algorithm for the velocity-pressure coupling has been applied (Patankar, 1980;

Versteeg and Malalasekera, 1995). After calculation of temperature and velocity fields as well as frost thickness, the overall heat transfer coefficient on the heat exchanger has been computed, according to equations (6)-(8). Subsequently, the instantaneous exchanged heat flux has been computed for every time step. The algorithm has been implemented in a self-written Fortran code and solved on a personal computer. When the calculation procedure reaches the end of the cooling period, the defrosting period has been simulated consequently. The calculation of heat needed for defrosting is based on the previously calculated amount of frost layer. The whole calculation procedure has been show in a block diagram on Fig. 5. The validation of the computational procedure has been performed by comparison of numerical results with experimental data. The validation has been performed by simulating several sets of experimental conditions. A detailed description of testing equipment and experimental validation has been given in (Lenic et al. 2008.; Lenic, 2006).

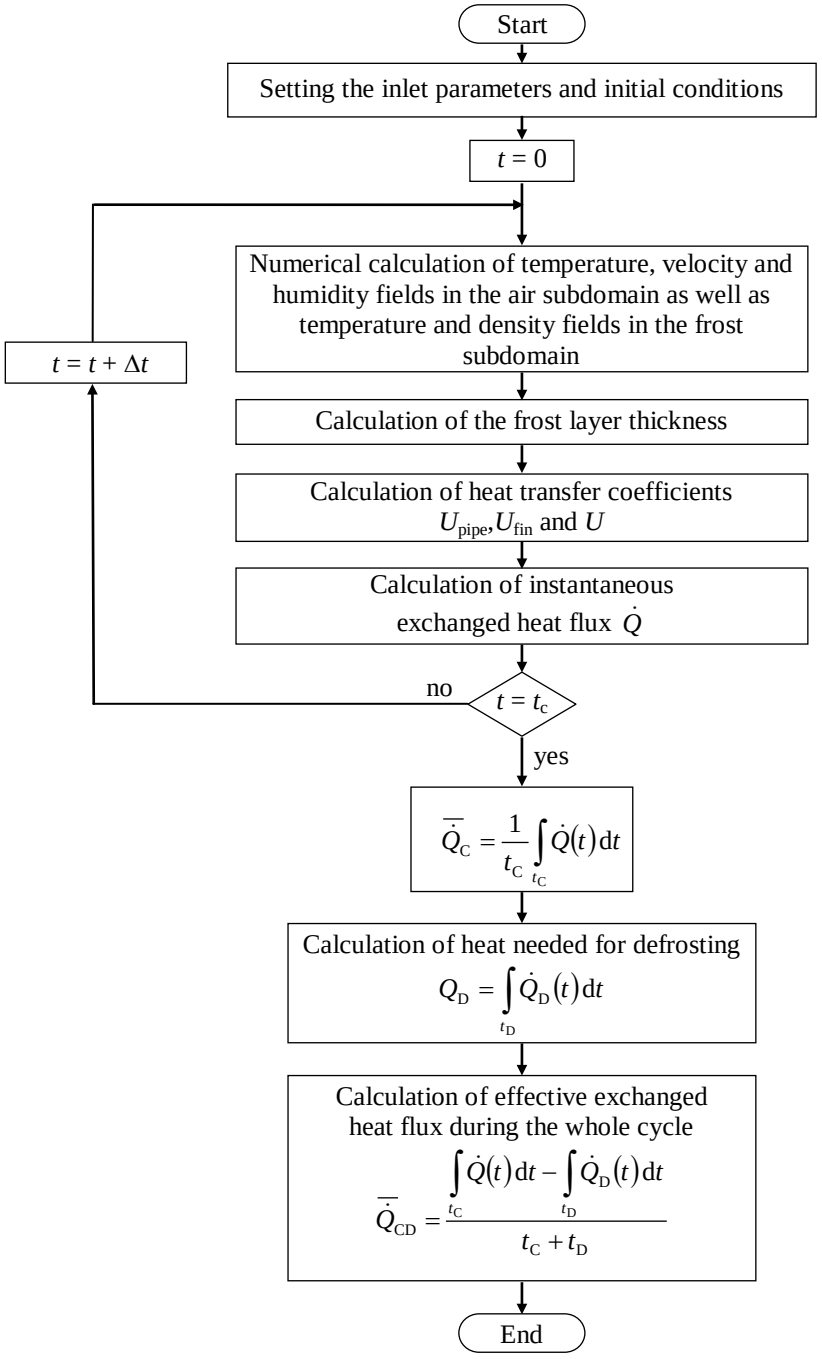

Figure 5. Block diagram for the calculation of the effective exchanged heat flux

Table 1. The overview of defrosting methods

Heat supply from refrigerant side (through the fins)				Heat supply from air side	
Hot gas refrigerant defrosting	Hot liquid refrigerant defrosting	Secondary pipe system	Electrical heating elements	Cold store air or hot air	Spraying with water or brine

4. CALCULATION RESULTS

4.1. Instantaneous exchanged heat flux

The calculation has been performed for the fin-and-tube heat exchanger with the following geometrical characteristics: fin thickness 0.001 m, space between fins 0.006 m, fin width 0.048 m, total number of pipes 189, total number of fins 210, heat exchanger surface 18 m^2, longitudinal pipe distance 0.016 m, transversal pipe distance 0.014 m, outer pipe diameter 0.01 m and inside pipe diameter 0.008 m. A set of numerical calculations has been performed in order to evaluate the influence of operating conditions on instantaneous exchanged heat flux. The results of many calculations have shown that the influence of air humidity on frost layer growth rate and thus on instantaneous exchanged heat flux is substantial. Time-wise variations of instantaneous and nominal heat flux ratio during frost formation for different inlet air humidities are shown on Fig. 6. Nominal heat flux is exchanged when all fins and pipes of the heat exchanger are clean, i.e. without any frost layer. If the heat exchanger operates in frost growth conditions, as a result of additional thermal resistance, the exchanged heat flux will be lower. Frost layer growth is more intensive under higher air humidities because of the higher gradient of air humidity near the frost surface in the boundary layer. Consequently, higher frost growth rates lead to an intensive decrease of the exchanged heat flux. For example, if the inlet air humidity is 2 g/kg, after three hours of operation, the exchanged heat flux is reduced by about 28 % regarding nominal heat flux. If the inlet air humidity is higher, for example 4 g/kg, 36 % heat flux reduction occurs.

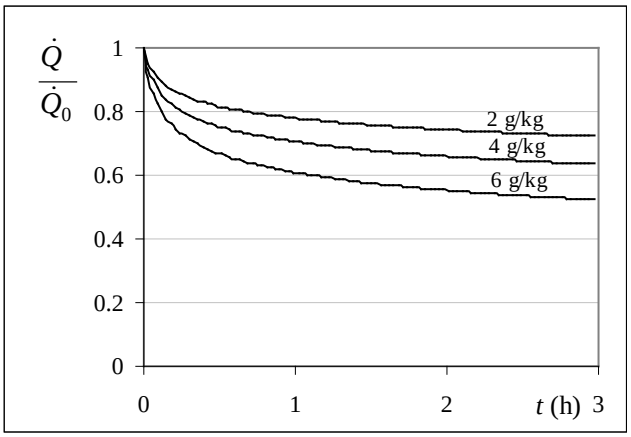

Figure 6. Time-wise variations of instantaneous and nominal heat flux ratio during frost formation for different air humidities ($T_{a,in}$ = 12 °C, $u_{x,in}$= 1 m/s, T_{fs} = -12 °C)

4.2. Different duration of the cooling period

It is not always easy to choose correctly the starting moment of the defrosting cycle. The defrosting process is an energy consumption process. Moreover, it causes the discontinuous

production of cooling energy since the device does not produce any cooling output during defrosting periods. Therefore, it is important to perform the defrosting process only when it is really necessary. The frequency of defrosting cycles is usually preset i.e. the device runs a defrosting cycle after some period of working time, regardless of the real frosting condition. During such an operating mode, some too large or too short cooling periods might be unwontedly obtained. The cooling period could have an inadequate duration, considering optimal energy consumption and adequate cooling power supply. If the device works under operating conditions which are favourable for frost layer growth, in some cases of intensive frost growth, too large cooling periods might be obtained. This leads to a decrease of the mean exchanged heat flux under the tolerable limit, Fig. 7a. From the other side, too short cooling periods lead to a decrease of the mean exchanged heat flux also, because in this case the defrosting cycles have been performed too frequently, Fig 7b. Furthermore, frequent performing of the defrosting cycle causes unwanted break-downs of the cooling supply.

For the above-mentioned reasons, the importance of selecting the optimal duration of a cooling period is evident. Optimal duration of a cooling period will provide the best possible cooling output considering, at the same time, rational energy consumption.

Bearing in mind this primary aim, the simulation of a heat exchanger acting as an evaporator has been investigated numerically. The operation of a heat exchanger has been simulated for different cycle durations, different heat fluxes supplied during the defrosting process and for a variety of operating conditions. Only part of the results has been presented. Variations of exchanged heat flux during operation under different operating conditions and for different cycle duration have been evaluated. The time-wise exchanged heat flux variations for different cycle durations of 1, 2 and 3 hours and for constant defrosting heat flux of 0.6 kW have been shown on Fig. 8. The defrosting heat flux has been denoted as a negative value on a vertical axis. For the presented operating conditions, when shorter cycles are applied, the average exchanged heat flux of cooling period and the average exchanged heat flux of whole cycle are higher in comparison with cases when longer cycles have been used.

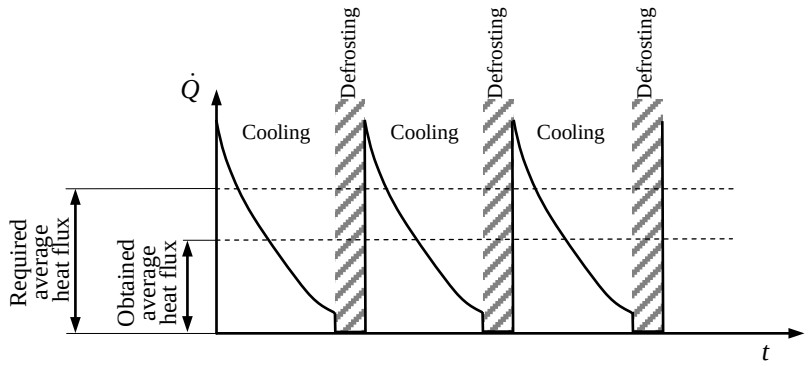

(a)

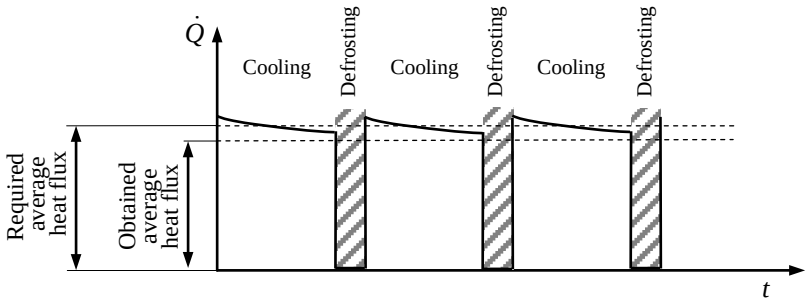

(b)

Figure 7. Too large (a) and too short (b) cooling periods

4.3. Optimal duration of a cooling period

Some recent experimental investigations have shown that the overall efficiency of the refrigeration device could be changed for 10-15% by manual adjustments of various operating parameters relating to the defrosting cycle. One of the investigated parameter was the temperature of the refrigerant used for defrosting, which influences the defrosting duration. The second influencing parameter was defrosting frequency. The aim of the analysis presented in this paper is to provide a controlling algorithm where the defrosting frequency will be defined by actual frosting conditions instead of preset periods of working time. Results obtained just offer a possible solution to the problem. Using the developed computer program, it is possible to set optimal duration of the cooling cycle, depending on operating parameters such as air humidity, air temperature, fin temperature and air velocity. By analyses of several cases with different operating parameters, the analytical correlations have been obtained. The correlations can be used for prediction of necessary duration of the cooling period depending on required average heat flux during the cooling cycle. With such correlations it is possible to determine the starting moment of the defrosting cycle.

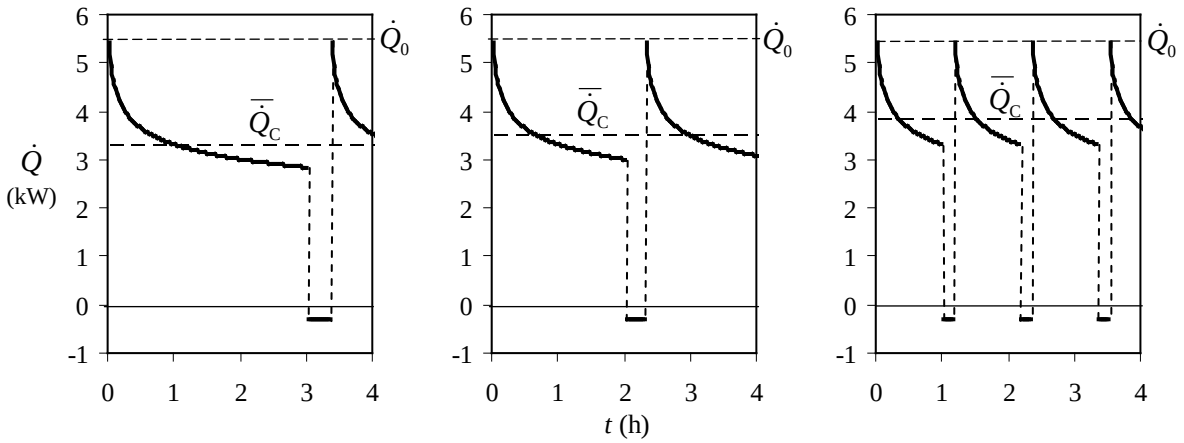

Figure 8. The time-wise exchanged heat flux variations during operation for different duration of the cooling cycle ($\dot{Q}_D = 0.6$ kW , $u_{x,in}$ = 1 m/s, $T_{a,in}$ = 12 °C, T_{fs} = -12 °C, w_{in} = 6 g/kg): (a) t_C=3 h; (b) t_C=2 h; (c) t_C=1 h

Hereafter, a few examples of implementation of the results have been presented in the form of diagrams. A diagram for the estimation of the maximally allowed duration of the cooling period depending on desired effective cooling output i.e. depending on the ratio of average and nominal exchanged heat flux, has been shown on Fig. 9. The results shown on the diagram have been calculated for different air humidities with defined values of air velocity, air temperature and fin temperature. For required average heat flux, the longest duration of cooling period can be determined, based on real frost growing conditions.

For example, if required average heat flux should amounts 70 % of the nominal heat flux, the period of cooling could last a maximum of 3 hours, when air humidity amounts 4 g/kg. If the air humidity is higher and amounts 6 g/kg, the period of cooling have to be shorter and the defrosting cycle should be applied after 1 hour of interrupted cooling operation. In this second case, the period of cooling should be shorter because higher air humidity causes intensive growth of frost layer as well as a reduction of the exchanged heat flux on a heat exchanger. Moreover, the defrosting cycles have to be performed more frequently.

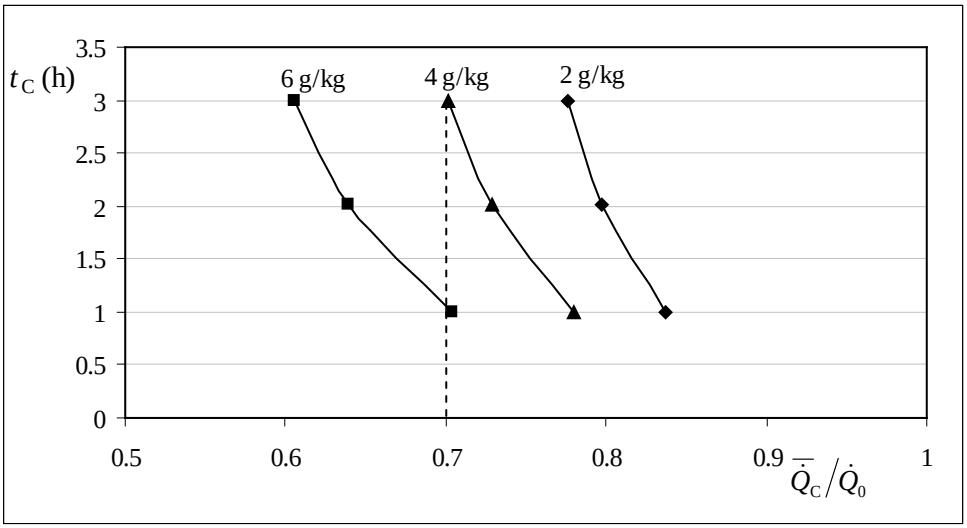

Figure 9. Maximally allowed duration of the cooling period depending on required ratio of average and nominal exchanged heat flux for different air humidities ($u_{x,in}$ = 1 m/s, $T_{a,in}$ = 12 °C)

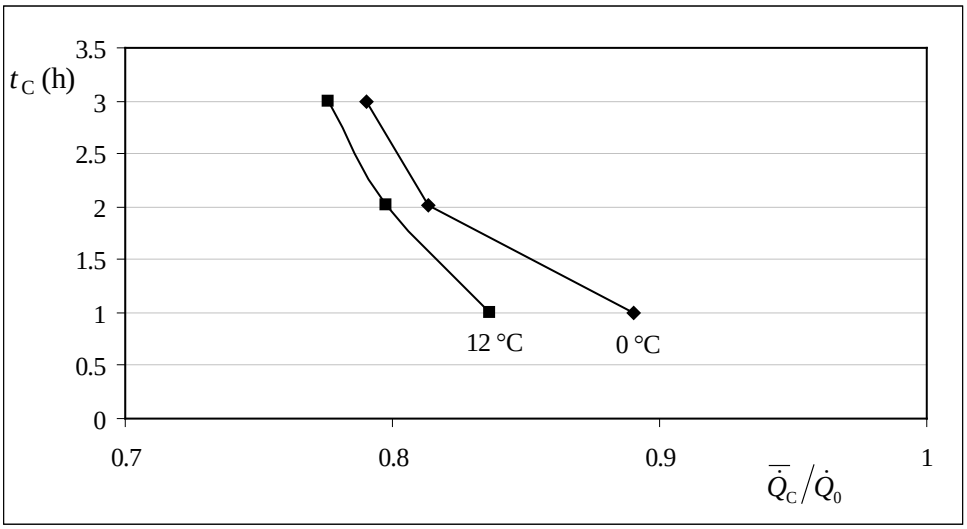

Figure 10. Maximally allowed duration of the cooling period depending on required ratio of average and nominal exchanged heat flux for different air temperatures ($u_{x,in}$ = 1 m/s, w_{in} = 2 g/kg)

The influence of air temperature has been also analysed. A diagram which can be used for selection of the maximally allowed duration of the cooling period for different air temperatures and for the air humidity of 2 g/kg has been presented on Fig. 10. The maximally allowed duration of the cooling period can be selected depending on required ratio of average and nominal exchanged heat flux. It can be noted that it is possible to obtain longer cooling periods under the lower air temperatures as opposed to the case with higher air temperatures. That is because the process of frost formation has been more intensive under operating conditions with higher air temperature, in the specific temperature range. If required average heat flux should amounts 80 % of the nominal heat flux, i.e. $\overline{\dot{Q}}_C/\dot{Q}_0 = 0.8$, the maximally allowed duration of cooling period is 2 hours with air temperature of 12 °C. If the air temperature is 0 °C, under the same other operating conditions, the allowed duration of cooling period can be 2.6 hours. Hence, in presented case, it is possible to obtain 0.6 hours longer cooling period if air temperature has been reduced by 12 degrees. This influence of air

temperature on maximally allowed duration of cooling period is not as significant as the influence of the air humidity.
The influence of air velocity on maximally allowed duration of cooling period for given heat flux ratio has been shown on Fig. 11. The diagram has been given for operating conditions with air humidity 4 g/kg and inlet air temperature of 12 °C. For the analysed operating conditions, the influence of air velocity is practically insignificant.

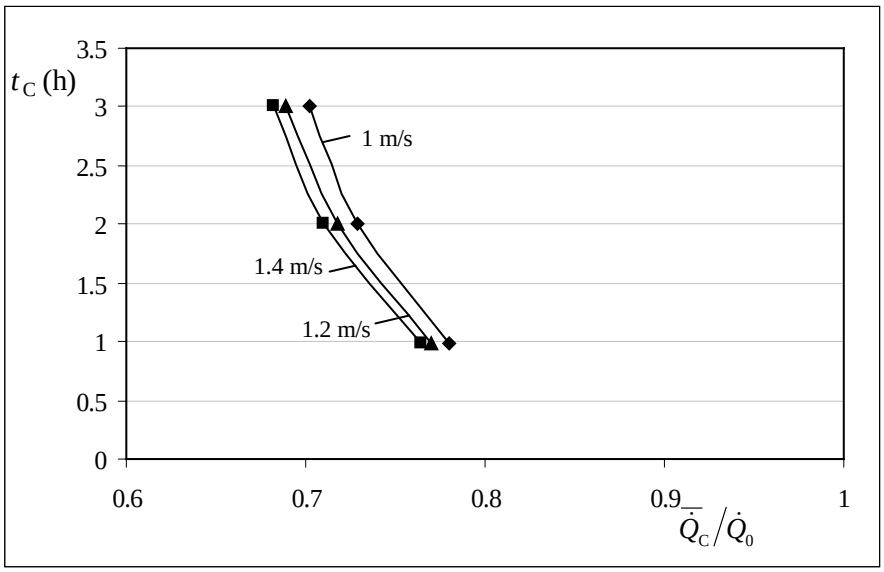

Figure 11. Maximally allowed duration of the cooling period depending on required ratio of average and nominal exchanged heat flux for different air velocities
($T_{a,in}$ = 12 °C, w_{in} = 4 g/kg)

5. CONCLUSIONS

Using an algorithm presented in the paper, it is possible to control the operating cycles of the device in an optimal manner by monitoring the operating conditions. The algorithm allows determining the optimal duration of the cooling cycle, depending on required average heat flux. Accordingly, unnecessary defrosting cycles can be avoided as opposed to the case with preset time-initiated defrosting control method. Moreover, cooling periods with unacceptable reduced exchanged heat flux, caused by thicker frost layer, can be avoided too. By monitoring the real operating conditions, which can be continuously measured, it is possible to control the operating process in the optimal way, considering the electrical energy consumption, quality and stability of delivered cooling or heating output.
For this purpose, a two-dimensional mathematical model of heat and mass transfer on a fin- and tube heat exchanger has been developed. The calculation of exchanged heat flux on a heat exchanger has been performed by detailed calculation of frost thickness and density, as well as air velocity, humidity and temperature in the boundary layer. Several cases with different operating conditions have been analysed and the results have been used to define the correlations for determining the optimal duration of the cooling cycle. The developed mathematical model and self-written computer program can successfully be used to predict the real behaviour of chillers operating under frost forming conditions.

6. LIST OF SYMBOLS

ΔA_{fin} fin surface area of the elementary segment (m^2)
$\Delta A_{fl,fin}$ air side fin surface area of the elementary segment (m^2)
$\Delta \overline{A}_{fin}$ average area (between ΔA_{fin} and $\Delta A_{fl,fin}$) at the middle of frost layer thickness (m^2)
ΔA_{pipe} pipe surface area of the elementary segment (m^2)
$\Delta A_{fl,pipe}$ air side pipe surface area of the elementary segment (m^2)
$\Delta \overline{A}_{pipe}$ average area (between ΔA_{pipe} and $\Delta A_{fl,pipe}$) at the middle of frost layer thickness (m^2)
ΔA_R refrigerant side pipe surface area (m^2)
a coefficient in linearised relationship of saturated air enthalpy and air temperature ($h_{sat,T} = a \cdot T + b = 1.4204 \cdot T + 10.205$) (J kg^{-1} K^{-1})
c_p specific heat capacity under a constant pressure (J kg^{-1} K^{-1})
D mass diffusivity (m^2 s^{-1})
h convective heat transfer coefficient (W m^{-2} K^{-1})
k thermal conductivity (W m^{-1} K^{-1})
l length (m)
m mass (kg)
$\dot{m}$ water vapour mass flux (kg m^{-2} s^{-1})
$\dot{m}_a$ water vapour mass flux from air towards frost layer (kg m^{-2} s^{-1})
p pressure (Pa)
Q heat (J)
$\dot{Q}$ heat flux (W)
q specific heat (J kg^{-1})
S supersaturation degree
s distance between fins (m)
T temperature (°C)
t time (s)
U overall heat transfer coefficient (W m^{-2} K^{-1})
u_x x-velocity component (m s^{-1})
u_y y-velocity component (m s^{-1})
W specific thermal resistance (m^2 K W^{-1})
w mass fraction of water vapour in air (kg kg^{-1})
x coordinate (m)
y coordinate (m)

Greek symbols

ε porosity
η efficiency
μ dynamic viscosity (Pa s)
ρ density, kg m^{-3}

Subscripts

a air
C cooling period
CD cooling-defrosting period
D defrosting period
diff related to diffusion into frost layer
eff effective

$_{fin}$ related to fin
$_{fl}$ frost layer
$_{fs}$ frost surface
$_{i}$ ice
$_{min}$ minimal
$_{mt}$ melting
$_{pipe}$ related to pipe
$_{R}$ refrigerant side
$_{s}$ fin surface
$_{in}$ inlet
$_{sat}$ saturated
$_{sub}$ sublimation
$_{tot}$ total
$_{v}$ water vapour
$_{\Delta y}$ related to layer thickness increasing
$_{0}$ initial value, nominal value
$_{1}$ inlet side
$_{2}$ outlet side
$_{\infty}$ free air stream

Superscripts
^{0} value at the beginning of the process
$^{-}$ average value

REFERENCES

[1] Sanders, C. T., *The influence of frost formation and defrosting on the performance of air coolers*, Ph.D thesis, Delft Technical University, Delft, 1974.
[2] Lenic, K., Trp, A., Frankovic, B., *Transient two-dimensional model of frost formation on a fin-and-tube heat exchanger*, Heat Mass Transfer , 52 (2009) 1-2, 22-32.
[3] Hayarishi, Y., Aoki, A., Adachi, S., Hori, K., *Study of frost properties correlating with frost formation types*, Journal of Heat Transfer 99 (1977), 239-245.
[4] Lee, K. S., Kim, W. S., Lee, T. H., *A one-dimensional model for frost formation on a cold surface*, International Journal of Heat and Mass Transfer 40 (1997), 4359-4365.
[5] Le Gall, R., Grillot, J. M., Jallut, C., *Modelling of frost growth and densification*, International Journal of Heat and Mass Transfer 40 (1997), 3177-3187.
[6] Lenic, K., *Analysis of heat and mass transfer during frost formation on fin-and-tube heat exchangers*, Ph.D. thesis, Faculty of Engineering University of Rijeka, Rijeka, Croatia, 2006 (in Croatian).
[7] Tao, Y. X., Besant, R. W., Reykallah, K. S., *A mathematical model for predicting the densification and growth of frost on a flat plate*, International Journal of Heat and Mass Transfer 36 (1996), 353-363.
[8] Lee, K., Jhee, S., Yang, D., *Prediction of the frost formation on a cold flat surface*, International Journal of Heat and Mass Transfer 46 (2003), 3789-3796.
[9] Jones, B. W., Parker, J. D., *Frost formation with varying environmental parameters*, Journal of Heat Transfer 97 (1975), 255-259.
[10] Sahin, A. Z., *An analytical study of frost nucleation and growth during the crystal growth period*, Heat and Mass Transfer 30 (1995), 321-330.
[11] Na, B., Weeb, R. L., *New model for frost growth rate*, International Journal of Heat and Mass Transfer 47 (2004), 925-936.

[12] Na, B., Weeb, R. L., *Mass transfer on and within a frost layer*, International Journal of Heat and Mass Transfer 47 (2004), 899-911.
[13] Sherif, S. A., Raju, S. P., Padki, M. M., Chan, A. B., *A semi-empirical transient method for modelling frost formation on a flat plate*, ASME Heat Transfer Div. 139 (1990), 15-23.
[14] Yang, D.K., Lee, K.-S., *Modelling of frosting behaviour on a cold plate*, International Journal of Refrigeration 28 (2005), 396–402.
[15] Cheng, C. H., Shiu, C. C., *Frost formation and frost crystal growth on a cold plate in atmospheric air flow*, International Journal of Heat and Mass Transfer 45 (2002), 4289–4303.
[16] Yang, D. K., Lee, K.S., Cha, D. J., *Frost formation on a cold surface under turbulent flow*, International Journal of Refrigeration 29 (2006), 164–169.
[17] Yang, D. K., Lee, K. S., Song, S., *Modelling for predicting frosting behaviour of a fin–tube heat exchanger*, International Journal of Heat and Mass Transfer 49 (2006), 1472–1479.
[18] Tso, C. P., Cheng, Y. C., Lai, A. C. K., *An improved model for predicting performance of finned tube heat exchanger under frosting condition with frost thickness variation along fin*, Applied Thermal Engineering 26 (2006), 111–120.
[19] Mago, P. J., Sherif, S.A., *Frost formation and heat transfer on a cold surface in ice fog*, International Journal of Refrigeration 28 (2005), 538–546.
[20] Lee, Y. B., Ro, S. T., *Analysis of the frost growth on a flat plate by simple models of saturation and supersaturation*, Experimental Thermal and Fluid Science 29 (2005), 685–696.
[21] Patankar, S. V., *Numerical Heat Transfer and Fluid Flow*, Hemisphere Publishing Corporation, Taylor & Francis Group, New York, 1980.
[22] Versteeg, H. K., Malalasekera, W., *An Introduction to Computational Fluid Dynamics: The Finite Volume Method*, Longman Scientific and Technical, Essex, 1995.

MOGUĆNOST ADAPTIVNOG UPRAVLJANJA PROCESOM HLAĐENJA I RAZLEĐIVANJA U OVISNOSTI O UVJETIMA NASTANKA LEDENOG SLOJA NA ISPARIVAČU

Sažetak: *U radu je provedena analiza rada uređaja u uvjetima nastanka ledenog sloja na isparivaču topline. Rezultati numeričkog rješavanja matematičkog modela izmjene topline i tvari u graničnom sloju, korišteni su kao temelj za proračun efektivnog izmijenjenog toplinskog toka u isparivaču. Analizirano je nekoliko slučajeva različitih ulaznih pogonskih parametara što je rezultiralo određivanjem korelacija kojima se može odrediti optimalno trajanje ciklusa hlađenja. Predstavljeni rezultati mogli bi se iskoristiti kao pomoć pri upravljanju uređaja u svrhu boljeg iskorištenja rashladnog učinka uređaja. U predloženom algoritmu, prilikom upravljanja uređajem, početni trenutak procesa razleđivanja određuje se temeljem trenutnih pogonskih uvjeta kao što su temperatura, vlažnost i brzina zraka te površinska temperatura isparivača.*

Ključne riječi: lamelni izmjenjivač topline, proces razleđivanja